DOI: 10.61782/fa.2025.0100

FORUM ACUSTICUM
EURONOISE 2025

ADAPTIVE 3D PLANE WAVE IMAGING THROUGH INTERFACES

Guillermo Cosarinsky[1*] **Adrián Rubio**[1,2] **Mario Muñoz**[1,2]
Jorge F. Cruza[1] **Jorge Camacho**[1]

[1] Ultrasound Systems and Technology Group (GSTU), Institute for Physical and Information Technologies (ITEFI), Spanish National Research Council (CSIC), c/Serrano 144, 28006 Madrid, Spain

[2] Electronics Department, Escuela Politécnica, Universidad de Alcalá de Henares, Ctra.Madrid-Barcelona, Km. 33,600, 28805 Madrid, Spain

ABSTRACT

Plane Wave Imaging (PWI) with ultrasonic arrays, initially developed for fast medical imaging, is nowadays being applied in Ultrasonic Testing (UT) for Non-Destructive Testing (NDT). In NDT, the Total Focusing Method (TFM) is regarded as the gold standard for image quality. However, TFM requires multiple transmission events (one for each array element), which can be slow for applications demanding very fast image acquisition. Since PWI can generate images of comparable quality with fewer transmissions, it presents a promising solution for such high-speed applications. This study demonstrates how volumetric PWI can be achieved using matrix arrays for testing arbitrarily shaped components, where a coupling medium is required and ultrasound waves are refracted on the component surface. This introduces complexity in calculating the time delays required to generate a plane wave within the component, a process that is straightforward in a single propagation medium scenario. Additionally, since the computation of those delays requires knowledge of the surface shape, we also explore how plane waves can be utilized for fast estimation of the surface shape.

Keywords: *non-destructive testing, plane wave imaging, adaptive imaging, matrix arrays*

**Corresponding author*: *g.cosarinsky@csic.es.*

1. INTRODUCTION

Non-Destructive Testing (NDT) plays a crucial role in ensuring the safety and integrity of critical infrastructure. In recent years, Plane Wave Imaging (PWI) has emerged as a promising technique for ultrasonic testing, offering significant advantages over traditional methods in terms of speed and image quality. Originally developed for medical imaging applications [1], PWI has found increasing relevance in industrial NDT scenarios, where rapid inspection and high-resolution imaging are fundamental [2].

In the field of NDT, the Total Focusing Method (TFM) has long been considered the gold standard for image quality [3]. However, TFM's requirement for multiple transmission events—one for each array element—can be a limiting factor in applications that demand very fast image acquisition. This limitation becomes significant when image reconstruction is performed by software and RF signals must be transferred to a computer, creating a bottleneck. Plane Wave Imaging (PWI) addresses this issue by reducing the amount of data that needs to be transferred and processed, generating images of comparable quality to TFM.

The application of PWI in industrial settings, particularly for testing components with complex geometries, presents unique challenges. Unlike medical applications where ultrasound typically propagates through a single medium, industrial NDT often involves coupling media and refraction at component surfaces. This introduces complexity in calculating the time delays required to generate a plane wave within the inspected component, a process that is relatively straightforward in single-medium

scenarios.

These challenges were addressed for the case of linear arrays and 2D imaging by various works [4–6]. In the context of railway inspection, Chang et al. [7] demonstrated a wavenumber-domain PWI technique capable of real-time dynamic imaging in vibrating environments, achieving frame rates of up to 83.3 fps. These developments highlight the potential of PWI to revolutionize NDT practices in the railway industry and beyond.

This study aims to further advance the application PWI using matrix arrays to perform 3D imaging of arbitrarily shaped components. We present a method for computing delay laws in 3D, which introduces additional challenges compared to the 2D case. Furthermore, we explore the use of plane waves for the rapid estimation of surface shape, a crucial step in accurately calculating time delays for wave generation within the component. The proposed methods are demonstrated through an example involving the testing of a cylindrical test piece using a 3 MHz 11x11 array.

2. METHODS

In this section we derive the emission focal laws to generate a three-dimensional plane wave across any given surface using a two-dimensional array. The approach begins by identifying a central ray originating from the array's center and refracting it in the desired plane wave direction, determined via Snell's law. For the remaining array elements, Fermat's principle is employed to compute rays that converge to a far-field focus positioned along the previously calculated central ray. A step-by-step derivation is provided below.

Figure 1 illustrates the geometry involved. A plane wave can be defined by a unit direction vector $\hat{k}$. For each array element E a ray must be found that refracts in the plane wave direction. To this end, the corresponding entry point G must be found (Figure 1.a). Snell's law states that the incident ray, the surface normal $\hat{n}$ at G, and the refracted ray are contained in a plane called the incidence plane. The directions of the incident and refracted rays are given by the unit vectors $\hat{v}_1$ and $\hat{v}_2$ respectively (Figure 1.b). According to Snell's law:

$$c_2 \sin(\theta_1) = c_1 \sin(\theta_2) \tag{1}$$

where θ_1 is the incidence angle, θ_2 the refraction angle, and c_1, c_2 the wave propagation velocities of the two media.

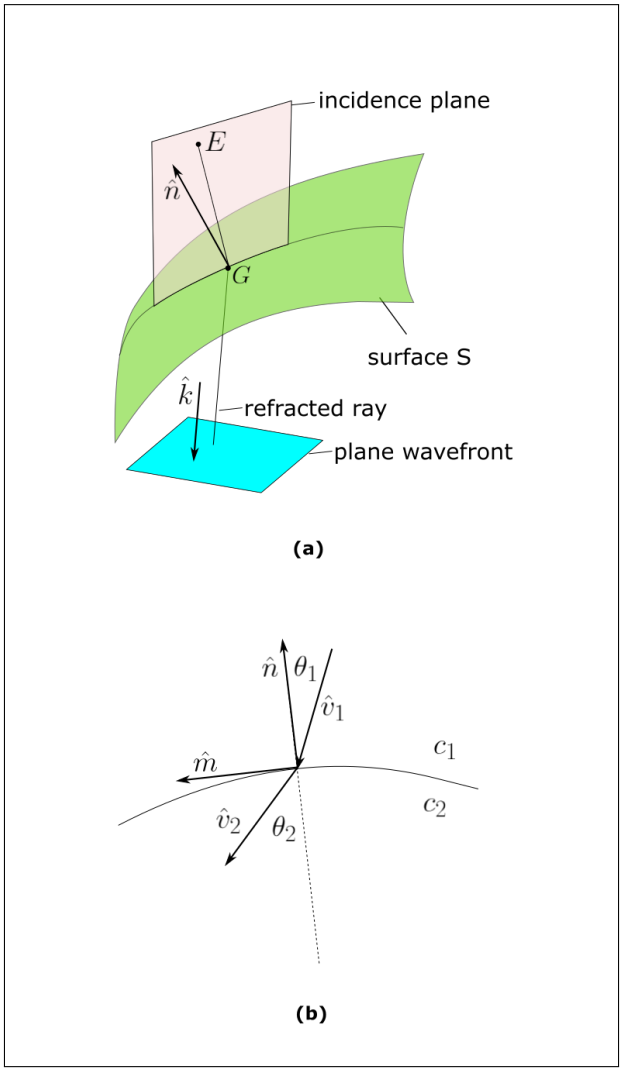

Figure 1. Geometry involved in the generation of a 3D plane wave through refraction. (a) Test piece surface, incidence plane and wavefront. (b) Vectors for Snell's law calculations

Given an element E and an entry point G, the incident unit vector is $\hat{v}_1 = \frac{\overline{EG}}{\|\overline{EG}\|}$. We need to compute $\hat{v}_2$ as a function of G, and solve the equation $\hat{v}_2 = \hat{k}$. From Figure 1.b we can see that:

$$\hat{v}_2 = \sin(\theta_2)\hat{m} - \cos(\theta_2)\hat{n} \tag{2}$$

where $\hat{m}$ is a tangent vector contained in the incidence

plane, which is given by:

$$\hat{m} = \hat{v_1} - \hat{v}_1 \cdot \hat{n} \tag{3}$$

The incidence angle cosine is given by the dot product:

$$\cos(\theta_1) = -\hat{v}_1 \cdot \hat{n} \tag{4}$$

Using equations (1) and (4) we get:

$$\sin(\theta_2) = \frac{c_2}{c_1}\sqrt{1 - (\hat{v}_1 \cdot \hat{n})^2} \tag{5}$$

Equations (2) and (5) along with the relation $\cos(\theta_2) = \sqrt{1 - \sin^2(\theta_2)}$ gives us $\hat{v}_2$ as a function of $\hat{v_1}$ and $\hat{n}$:

$$\hat{v}_2 = \frac{c_2}{c_1}\sqrt{1 - (\hat{v}_1 \cdot \hat{n})^2}\,(\hat{v_1} - \hat{v}_1 \cdot \hat{n}) - \sqrt{1 - \left(\frac{c_2}{c_1}\sqrt{1 - (\hat{v}_1 \cdot \hat{n})^2}\right)^2}\,\hat{n} \tag{6}$$

As was said before, to find the entry point coordinates (x, y, z) we should solve $\hat{v}_2 = \hat{k}$, which is a system of three non-linear equations. However, the z coordinate is a dependent variable. We suppose the surface is represented by a function $z = f(x, y)$. Additionally, vectors $\hat{v}_2$ and $\hat{k}$ have unit norm and thus one of its three coordinates is dependent on the other two. Therefore, we have a system of two equations with the two unknowns (x, y). Equation (6) does not show explicitly the dependence on (x, y). In order to make it explicit we should express the coordinates of $\hat{v_1}$ and $\hat{n}$ in terms of (x, y) as:

$$\hat{v}_1 = \frac{(x - E_x, y - E_y, f(x, y) - E_z)}{\sqrt{(x - E_x)^2 + (y - E_y)^2 + (f(x, y) - E_z)^2}} \tag{7}$$

$$\hat{n} = \frac{(-\frac{\partial f}{\partial x}, -\frac{\partial f}{\partial y}, 1)}{\sqrt{1 + \frac{\partial f}{\partial x}^2 + \frac{\partial f}{\partial y}^2}} \tag{8}$$

where (E_x, E_y, E_z) are the array element coordinates. Replacing (7) and (8) in (6) to solve $\hat{v}_2 = \hat{k}$ results in a complex and cumbersome system of equations with no analytical solution. As in the 2D case, numerical methods are needed to solve it. Newton-Raphson method might be used, but it required the calculation expression (6) partial derivatives which gives lengthy and impractical formulae. Thus, we implemented a brute force grid search approach, which is inefficient but easy to implement. We will call this method of computing the entry point Brute Force Snell (BFS). If it has to be applied to all the array elements, the overall computation time would be very high.

An alternative method for the computations of the entry points can be derived by following this idea: a plane wave emission is equivalent to an emission focused to a point in infinity. This is illustrated in Figure 2.a, where a bunch of rays from array elements is refracted and focused to a point F_{far} very distant to the array and surface. Figure 2.b shows the bunch of rays is close to a bunch of parallel rays. Rays from the array elements to F_{far} can be computed using Fermat's principle. But first we need to find the appropriate F_{far} for a given plane wave direction $\hat{k}$. As show in Figure 2.b, the far away focus must be located on the ray coming from the array center O_P, that is refracted at the point G_P. Thus $\overline{G_P F_{far}} = s\hat{k}$ with $s >> W$, where W is the aperture size ($s = 100 * W$ for example). Entry point G_P must be computed by Snell's law. In our case that was done using BFS, which is a slow algorithm but its only applied once per plane wave.

The emission time delay $\Delta t(E)$ for an array element E is finally computed as:

$$\Delta t(E) = t(E, F_{far}) - t(O_P, F_{far}) \tag{9}$$

where $t(E, A)$ is the TOF from E to a point A. With these delays a plane wave is created such that it goes through the array center at time $t = 0$. The TOF $t_{PW}(\hat{k}, \vec{r})$ of the plane wave to a point A is finally computed as:

$$t_{PW}(\hat{k}, A) = t_{far} + \frac{1}{c_2}\overline{F_{far}A} \cdot \hat{k} \tag{10}$$

$$t_{far} = t(O_P, F_{far}) \tag{11}$$

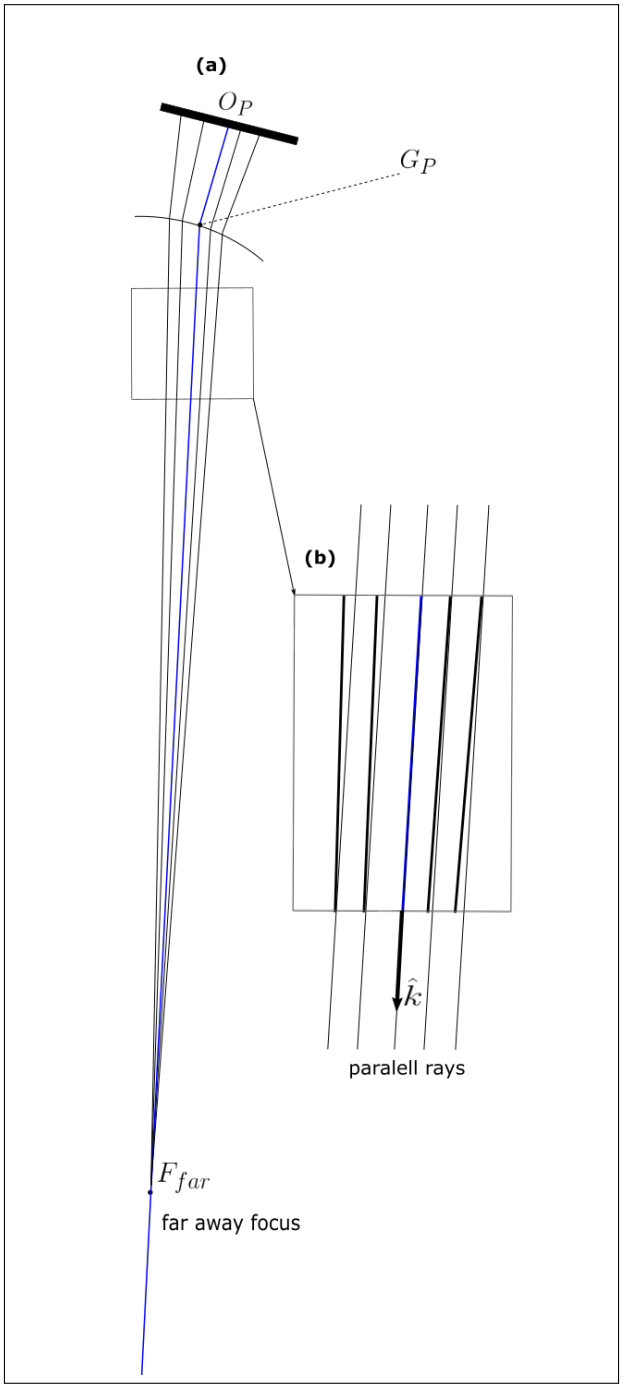

Figure 2. Geometry involved in the generation of a 3D plane wave through refraction. (a) Test piece surface, incidence plane and wavefront. (b) Vectors for Snell's law calculations

To compute the total TOF, we must calculate the ray path from the point $\vec{r}$ to each array element. This process typically requires an iterative calculation using Fermat's principle, which is computationally intensive. To optimize this procedure, we employ the 3D Virtual Array method, which we developed in our previous work [8].

As previously mentioned, TOF computations require a surface representation in the form $z = f(x, y)$. This representation can be obtained using ultrasound echoes reflected from the component's surface. In our previous work [9], we proposed several methods to achieve this for basic geometries, such as cylinders, planes and spheres.

One approach involves using a single plane wave directed along the array normal. This method has the advantage of requiring only a single firing, making it very fast. However, this method may fail if the probe's normal is at a significant angle to the surface, so it is best used in scenarios where such angular deviations are avoided.

For more complex or general geometries, alternative methods should be employed. Techniques such as those described in [10, 11] are promising candidates but would need to be extended to three-dimensional cases, as demonstrated in [12].

3. EXPERIMENTAL VALIDATION

In this section, we present an experimental example using a cylindrical aluminum test component with a 10 mm radius, featuring two Flat Bottom Holes (FBHs) in its midplane. The probe used was a 3 MHz, 11x11 matrix array with a 1 mm pitch. Data acquisition was performed using the SITAU II 128 full-parallel ultrasound system by DASEL S.L. (Spain).

TFM and PWI techniques were applied to generate images within a volume of 88x80x80 voxels. PWI was performed using nine plane waves, with an additional wave dedicated to surface detection. Lateral views of the resulting volumetric images are shown in Figure 3. It is observed in Figures 3 a and b that both methods produce similar results, where the 2 FBHs (H1 and H2 in Figure 3.a) are clearly imaged. A detailed comparison is presented in Figure 3.c, which displays the lateral amplitude profiles of H1 and H2, revealing that the contrast of H1 is slightly better in TFM. However, the acquisition efficiency difference between TFM and PWI is significant. TFM requires 121 individual firings, corresponding to each element in the 11x11 matrix array. In contrast, PWI in this experiment utilizes only 9 plane wave firings. Consequently, the RF signals collected for TFM contain ap-

proximately 14 times more data than those acquired for PWI. This substantial reduction in data volume for PWI highlights its potential for faster acquisition and processing times, which can be crucial in real-time imaging applications.

The main drawback of PWI is the requirement for an additional acquisition step to detect and reconstruct the surface, as well as the need to compute the emission focal laws—tasks that are unnecessary in the Full Matrix Capture (FMC) mode used for TFM, as they don't depend on the surface shape. However, in some cases, surface detection can be accomplished with just a single firing, and the computation of the delays, using the method described in Section 2, is highly efficient. In the example presented, this computation takes approximately 1 millisecond.

Regarding the software beamforming execution time, our current GPU implementation using an Nvidia GeForce RTX 3090 card demonstrates significant performance improvements for PWI compared to TFM: 68 ms for TFM and 15 ms for PWI. This represents more than a 4-fold speed increase for PWI over TFM in terms of image reconstruction. However, the most substantial advantage lies in the reduced data transfer time associated with PWI, coarsely 14 times less data in PWI than in TFM.

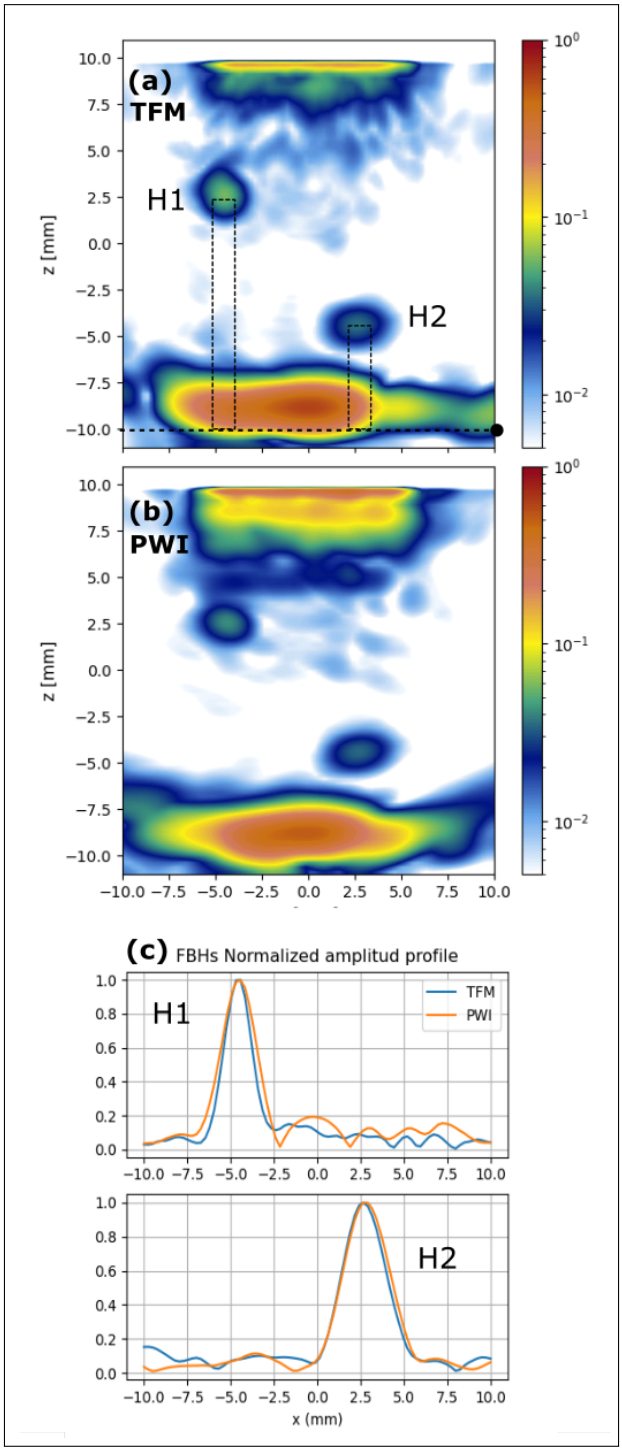

Figure 3. TFM and PWI images (lateral view). The cylinder axis is coincident with the X-axis. (a) TFM image; FBHs are represented by dashed lines in the schematic overlay (b) PWI image with 9 plane waves, (c) Amplitude profiles of the FBHs for the two imaging methods.

4. CONCLUSIONS

This study has demonstrated the feasibility and advantages of using 3D PWI with matrix arrays for non-destructive testing of components with arbitrarily shaped surfaces. By addressing the challenges associated with wave refraction at interfaces, we have presented a method for computing the delay laws required for the generation of plane waves within the inspected component. The use of a surface representation derived from ultrasound echoes makes the proposed method adaptive.

Experimental validation using a cylindrical test component with flat-bottom holes confirmed the effectiveness of the 3D PWI technique. The results demonstrate that PWI can achieve comparable image quality to the Total Focusing Method (TFM) while significantly reducing the number of transmission events.

Future work will focus on refining the surface detection and reconstruction algorithms and conducting comprehensive comparisons with TFM across a wider range of component geometries and defect types. Ultimately, the advancements in 3D PWI presented in this study contribute to the ongoing evolution of NDT techniques, paving the way for more efficient and reliable inspection of critical infrastructure components.

5. ACKNOWLEDGMENTS

This research was supported by the project PID2022-143271OB-I00, funded by MCIN/AEI /10.13039/501100011033/FEDER, UE., the project PLEC2024-011165, funded by MICIU/AEI/10.13039/501100011033/ FEDER, UE, and by the European Commission – NextGenerationEU, through Momentum CSIC Programme: Develop Your Digital Talent. The funding for these actions/grants and contracts comes from the European Union's Recovery and Resilience Facility-Next Generation, in the framework of the General Invitation of the Spanish Government's public business entity Red.es to participate in talent attraction and retention programmes within Investment 4 of Component 19 of the Recovery, Transformation and Resilience Plan.

G. Cosarinsky staff is hired under the Generation D initiative, promoted by Red.es, an organisation attached to the Ministry for Digital Transformation and the Civil Service, for the attraction and retention of talent through grants and training contracts, financed by the Recovery, Transformation and Resilience Plan through the European Union's Next Generation funds.

6. REFERENCES

[1] G. Montaldo, M. Tanter, J. Bercoff, N. Benech, and M. Fink, "Coherent plane-wave compounding for very high frame rate ultraso- nography and transient elastography," *IEEE Trans. Ultrason. Ferroelectr. Freq. Control*, vol. 56, pp. 489–506, 2009.

[2] L. Le Jeune, S. Robert, and C. Prada, "Plane wave imaging for ultrasonic inspection of irregular structures with high frame rates," in *AIP Conference Proc.*, vol. 1706, (Melville, NY, USA), p. 020010, AIP Publishing LLC, 2016.

[3] C. Holmes, B. Drinkwater, and P. Wilcox, "The post-processing of ultrasonic array data using the total focusing method," *Insight: Non-Destructive Testing and Condition Monitoring*, vol. 46, no. 11, pp. 677–680, 2004.

[4] G. Cosarinsky, J. F. Cruza, and J. Camacho, "Plane wave imaging through interfaces," *Sensors*, vol. 21, no. 15, 2021.

[5] R. Rachev, P. Wilcox, A. Velichko, and K. McAughey, "Plane wave imaging techniques for immersion testing of components with nonplanar surfaces," *IEEE Trans. Ultrason. Ferroelectr. Freq. Control*, vol. 67, pp. 1303–1316, 2020.

[6] H. Sui, P. Xu, J. Huang, and H. Zhu, "Space optimized plane wave imaging for fast ultrasonic inspection with small active aperture: Simulation and experiment," *Sensors (Switzerland)*, vol. 21, no. 1, pp. 1–11, 2021.

[7] Z. Chang, X. Xu, S. Wu, E. Wu, K. Yang, J. Chen, and H. Jin, "Ultrasonic dynamic plane wave imaging for high-speed railway inspection," *Mechanical Systems and Signal Processing*, vol. 220, p. 111672, 2024.

[8] G. Cosarinsky, J. F. Cruza, M. Muñoz, and J. Camacho, "Optimized auto-focusing method for 3d ultrasound imaging in ndt," *NDT and E International*, vol. 134, no. November 2022, 2023.

[9] G. Cosarinsky, J. F. Cruza, M. Muñoz, and J. Camacho, "Automatic estimation of surface and probe location for 3d imaging with bidimensional arrays," *NDT and E International*, vol. 141, p. 102990, 2024.

[10] J. Camacho, F. Cruza, J. Brizuela, and C. Fritsch, "Automatic dynamic depth focusing for ndt," *IEEE Trans. Ultrason. Ferroelectr. Freq. Control*, vol. 61, pp. 673–684, 2014.

[11] R. E. Malkin, A. C. Franklin, R. L. Bevan, H. Kikura, and B. W. Drinkwater, "Surface reconstruction accuracy using ultrasonic arrays: Application to non-destructive testing," *NDT and E International*, vol. 96, no. February, pp. 26–34, 2018.

[12] J. G. McKee, R. L. T. Bevan, P. D. Wilcox, and R. E. Malkin, "Volumetric imaging through a doubly-curved surface using a 2d phased array," *NDT E International*, vol. 113, no. August, p. 102260, 2020.